A model for biaxial fatigue limits

Alfredo Navarro, Carpoforo Vallellano, Victor Chaves, Carmen Madrigal

Departamento de Ingeniería Mecánica, Escuela Superior de Ingenieros, Universidad de Sevilla, Camino de los Descubrimientos s/n, 41092 Sevilla, Spain. E-mail: navarro@us.es

ABSTRACT. *This paper presents the extension to biaxial proportional loads of a short crack growth model based on the blocking of dislocations at grain boundaries. The model considers a small inclined crack and its associated plastic zones blocked in a grain boundary and within a plane biaxial stress field. Two distributions of dislocations are employed to account for the climb and glide components of displacements. The conditions for activation of dislocations sources in the neighbour grain are established and this leads to a biaxial limit criterion which reproduces the well-know Gough and Pollard ellipse.*

INTRODUCTION

Virtually all machine components are under cyclic multiaxial stresses and strains during normal operation. These conditions can arise from the intrinsic geometry of the component (*viz.* the presence of stress raisers or notches) or its being under multiaxial loads. The fact that most components can eventually undergo fatigue failure has stimulated much interest in understanding their response under such demanding conditions.

Gough *et al.* [1, 2] were among the pioneers in studying the phenomenon of multiaxial fatigue in a careful, extensive manner. Their research was prompted by the need to develop effective methods for designing power transmission shafts to be simultaneously subjected to rotational bending loads and torsional loads. In fact, the shaft calculation method in widest use today–and endorsed, for example, in the American shafting standard ANSI/ASME B106.1M-1985[3]–is clearly based on their experimental results.

Gough's group used a specially designed resonating machine capable of applying alternate bending and torsional loads, and allowing the mean stress for both types of loads to be controlled. They used ductile steels and cast iron typically employed by the aeronautical and automobile industries at the time (the 1950s), which they subjected to various thermal treatments in order to obtain a wide variety of microstructures including ferrite-pearlite, pearlite and spheroidal cementite. In this way, they prepared 14 different materials for testing. Also, they studied solid and hollow cylindrical specimens with and without stress raisers. As can be inferred from the more than 200 S-N experimental curves reported in a paper by these authors [2], they conducted quite comprehensive

tests. Thus, each material and specimen type were analysed for the stress range to be applied in order to obtain a given life value at seven different values of the bending-to-torsional stress ratio ($\pm f/\pm q$). Fatigue limits were determined by endurance testing on a minimum basis of 10^7cycles. Their results were reported in the form of curves in the $f-q$ plane. Figure 1 shows a typical curve. The experimental data points fitted two different equations defining an elliptical quadrant (solid line in the figure):

$$\frac{f^2}{b^2}+\frac{q^2}{t^2}=1 \tag{1}$$

and an elliptical arc (dashed line in the figure):

$$\frac{q^2}{t^2}+\frac{f^2}{b^2}\left(\frac{b}{t}-1\right)+\frac{f}{b}\left(2-\frac{b}{t}\right)=1 \tag{2}$$

where $\pm b$ is the bending fatigue limit and $\pm t$ the torsional fatigue limit.

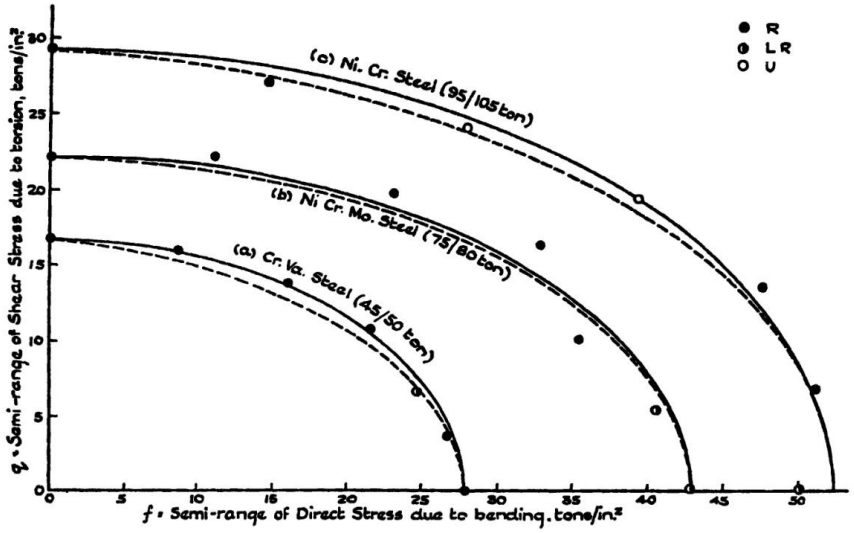

Figure 1.Typical experimental results of Gough et at. [2].

It should be noted that these equations are purely empirical in nature. In fact, they were based on static failure and yielding criteria, but modified in order to account for the fact that the experimentally determined tensile-to-torsional fatigue limit ratios for the studied materials consistently failed to comply with the predictions based on these static criteria; this led Gough's group to use such a ratio as an independent variable to be experimentally determined in each case (see [2, pp 35-40]). As noted by these authors, their aim was not to obtain the curve best fitting the seven experimental points available in each case; rather, they used the two extreme values of the experimental fatigue limits under pure bending and pure torsional loads in each case. The sole exception to this procedure was Cr-Ni steel, the curve for which is at the top of Figure 1.

The difference between the ellipse quadrant and ellipse arc depends on the b/t ratio. The two types of curve are very similar for materials with b/t ratios close to 2. The ratios for the materials studied by Gough *et al.* ranged from 1.1 for one cast iron to 1.93 for one of the most ductile steels used in specimens with no stress concentration. The

range spanned by notched specimens was 1.02-1.65. From their results, Gough *et al.* inferred that the behaviour of ductile materials was better fitted by an ellipse quadrant, and that of the most fragile materials and the notched specimens by an ellipse arc.

This paper describes the extension of a microcrack propagation model based on the theory of distribution of dislocations to the fatigue limit under biaxial loads. The following section provides an overview of this type of model.

MICROCRACK PROPAGATION MODEL. UNIAXIAL LOADING

Navarro and de los Ríos [4, 5] used the BCS concept to develop a model for fatigue propagation of microcracks in unnotched solids. It was assumed that plastic slip under fatigue conditions occurs in rectilinear slip bands across grains in the solid, and that cracks appear in those grains most readily forming persistent slip bands by effect of their size and crystallographic orientation. Also, they assumed that each crack and its associated plastic zone would expand just up to a microstructural barrier (usually a grain boundary), where it would be stopped until conditions for triggering plastic slip in the next grain were met. Crack propagation and blocking at a barrier would occur in each successive grain, and this introduces a certain discrete character into the theory, for the plastic zone does not advance in a continuous way; rather than that, it progresses by means of discrete jumps, engulfing a new grain each time it advances from barrier to barrier. This results in oscillating pattern of growth rate, with increasingly smaller amplitudes.

The crack, its plastic zones and barriers are represented by a continuous distribution of dislocations. Figure 2 shows a schematic depiction of the model, which assumes an infinite solid of a metal of average grain size D under a uniform stress τ and containing a crack of length $2a$ inside. The crack is assumed to have nucleated within a grain and its plastic zone to have grown over i grains (with $i = 1, 3, 5, \ldots$). In front of the crack tips are its associated plastic zones, which are blocked by the barriers at the end of a grain. The position of the grain boundary will be given by $iD/2$, which represents the number of half-grains crossed by the plastic zone on each side. The stresses $\sigma_1, \sigma_2, \sigma_3$ represent the resistance to dislocation movements in the crack, plastic zone and barrier, respectively. The microstructural barrier is modelled by a small zone of length r_0 ($r_0 \ll D$), which represents the typical size of the interface between grains or the typical distance to dislocation sources that can be activated in the next grain.

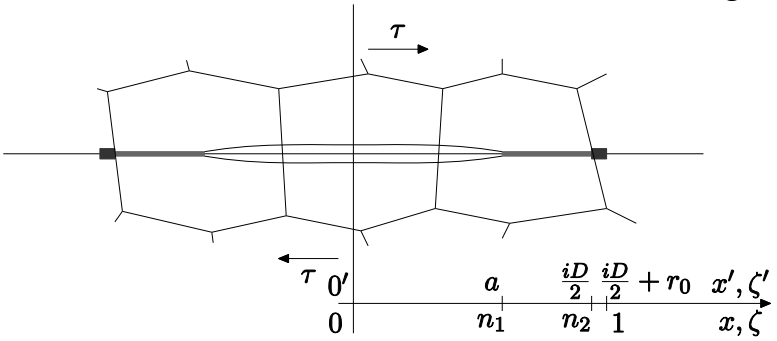

Figure 2. Crack, Plastic zone and barrier.

The relation describing the equilibrium of dislocations is an integral equation of the Cauchy type. On the constraint that the stress solution of the equation should be bounded throughout the field, one can obtain a relation to calculate the stress σ_3 at the barrier at any time. As the crack propagates, the stress σ_3 needed to maintain equilibrium increases and eventually peaks when the crack reaches the barrier. In the absence of interferences between the crack sides ($\sigma_1 = 0$) and for the crack tip exactly at the barrier edge ($n_1 = n_2 = (iD/2)/(iD/2 + r_0) \simeq 1$),

$$\sigma_3 = \frac{1}{\cos^{-1} n_2} \left[\frac{\pi}{2}\tau\right] \tag{3}$$

The crack will continue to propagate over another grain if the stress σ_3 reaches a critical value allowing the dislocation source to be activated. The critical activation condition can thus be expressed as follows:

$$\frac{\sigma_3}{m_i^*} = \tau_c \tag{4}$$

where m_i^* is a crystallographic orientation factor to project the stress σ_3 onto the plane and slip direction of a dislocation source in the adjacent grain, and τ_c is the critical stress needed to activate the source. The previous two equations allow one to calculate the minimum applied stress τ_{Li} required to activate plastic slip in the next grain. Using the approximation $\cos^{-1} n_2 = (2(1 - n_2))^{\frac{1}{2}} \approx 2(r_0/iD)^{\frac{1}{2}}$ one can obtain

$$\tau_{Li} = \frac{4}{\pi}\, m_i^* \tau_c \left(\frac{r_0}{iD}\right)^{\frac{1}{2}} \tag{5}$$

The fatigue limit, which following the nomenclature of Gough *et al.* used in the Introduction, is denoted by *t*, can be obtained by making $i = 1$ in the previous equation:

$$t = \tau_{L1} = \frac{4}{\pi}\, m_1^* \tau_c \left(\frac{r_0}{D}\right)^{\frac{1}{2}} \tag{6}$$

Obviously, τ_c and r_o are not measured in order to calculate t in practice; rather, the opposite procedure is used. Although this observation is seemingly trivial, it is the key to applying the model to more complex real-life problems such as those of notched elements. If one can relate the stress at the barrier with that applied upon the body, *i.e.*, if one can establish for the problem at hand the relation equivalent to Eq. (3) above, then the activation condition (Eq. (4)) can be modified by substituting the *microscopic* terms with the expressions relating them to the fatigue limit for the material (Eq. (6)) in order to derive an expression affording the calculation of the fatigue limit for a notched element as a function of the fatigue limit for the material [6-9].

EXTENSION TO PROPORTIONAL BIAXIAL LOADS

In the presence of proportional biaxial loads, one must consider two types of dislocation distributions, namely: one with Burgers vectors normal to the crack (climb) and the other with such vectors parallel to the crack (glide). Also, the crack propagation direction is unknown beforehand (see Figure 3). The tangential stress on the dislocation

sources now includes components from both dislocation sets. The activation condition allowing one to predict whether a crack will overcome its first barrier, which is the condition for the fatigue limit, is, thus, written:

$$\frac{\sigma_3}{m^*_{\sigma 1}} + \frac{\tau_3}{m^*_{\tau 1}} = \tau_c \tag{7}$$

where $m^*_{\sigma 1}$ and $m^*_{\tau_1}$ are the orientation factors allowing one to calculate the shear stress in the slip plane and the slip direction of the dislocation source from the stresses induced at the barrier by the two distributions of dislocations. We just assume that they add up to the total value.

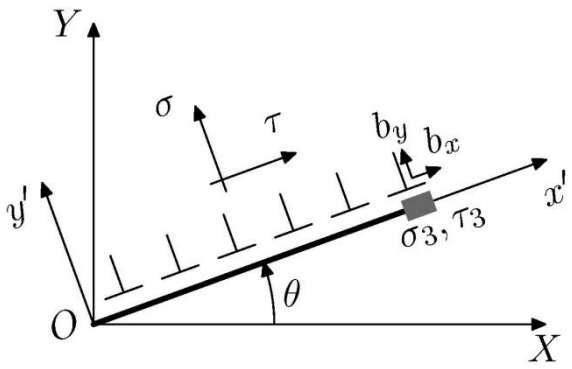

Figure 3. Model for Biaxial loading.

As with monoaxial loads, solving the equilibrium conditions for the two dislocation sets and using the existence condition for a bounded solution allows one to relate σ_3^1 and τ_3^1 at the barrier on the one hand, and σ and τ –which act in the crack plane– on the other. The ensuing relations are identical with Eq. (3), so the activation condition can be expressed as

$$\frac{1}{\cos^{-1} n_2}\frac{\pi}{2}\left[\frac{\tau}{m^*_{\tau 1}} + \frac{\sigma}{m^*_{\sigma 1}}\right] = \tau_c \tag{8}$$

which can be rewritten in a much more revealing form by using the approximation $\cos^{-1} n_2 = (2(1-n_2))^{\frac{1}{2}} \approx 2(r_0/iD)^{\frac{1}{2}}$ and rearranging:

$$\frac{\tau}{\tau_U} + \frac{\sigma}{\sigma_U} = 1 \tag{9}$$

where $\tau_U = \frac{4}{\pi}\, m^*_{\tau 1}\tau_c \left(\frac{r_0}{D}\right)^{\frac{1}{2}}$ and $\sigma_U = \frac{4}{\pi}\, m^*_{\sigma 1}\tau_c \left(\frac{r_0}{D}\right)^{\frac{1}{2}}$.

The previous relation is the equation of a straight line splitting the $\sigma - \tau$ plane in two regions (see Figure 4). Stress combinations above the line cause the activation of dislocation sources and hence cracks to propagate beyond their barriers and eventually result in failure. On the other hand, stress combinations below the line allow cracks to reach their barriers; however, because no plastic slip occurs beyond the barriers, cracks stop at them unless additional stress is applied.

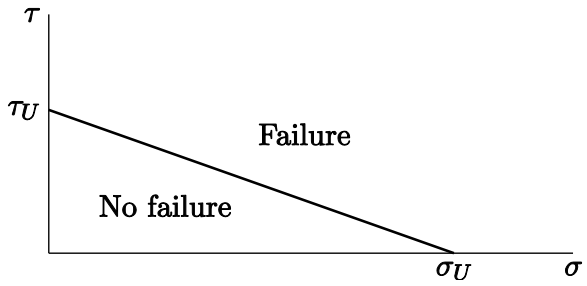

Figure 4. Biaxial Microscopic Activation Criterion (Eq. (9)).

Let us see how we can relate the microscopic properties of the material with the tensile and torsional fatigue limits via σ_U and τ_U. This can be easily achieved by examining the corresponding tests using Mohr's circle.

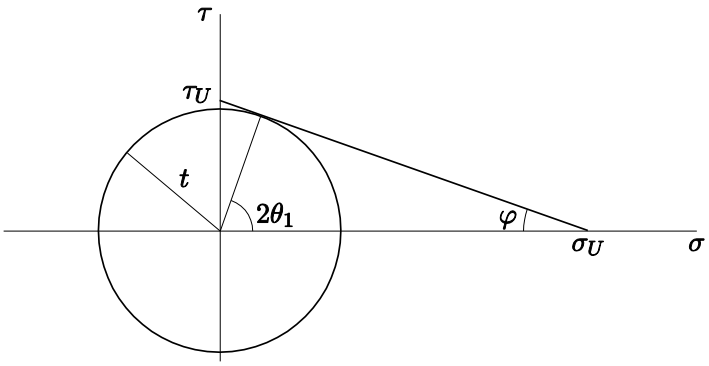

Figure 5. Morh Circle and Microscopic Activation Criterion for torsion.

Pure torsion test

Figure 5 shows Mohr's cycle for a pure torsion test. The material is subjected to fatigue in torsion. The maximum cyclic stress applied without fatigue failure (or, in other words, the minimum stress to be applied in order to cause failure) is obviously the torsional fatigue limit *t*. When the torsion stress applied in the test coincides with *t*, the Mohr cycle will be tangential to the line for the microscopic activation criterion.

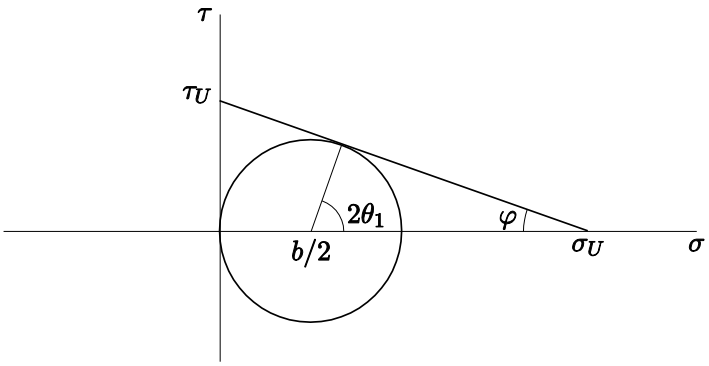

Figure 6. Morh Circle and Microscopic Activation Criterion for bending.

Pure bending test

Figure 6 shows the Mohr circle for a pure tensile test. The applied normal stress causing the Mohr circle to be tangential to the line for the microscopic criterion must be the bending fatigue limit, which is denoted by *b*.

Based on the previous two figures, one can readily obtain the following relations to calculate σ_U and τ_U from the tensile and torsional fatigue limits (b and t, respectively, with $\overline{\alpha} = b/t$):

$$\sigma_U = \frac{b}{2-\overline{\alpha}} \qquad \tau_U = \frac{b}{2\sqrt{\overline{\alpha}-1}} \tag{10}$$

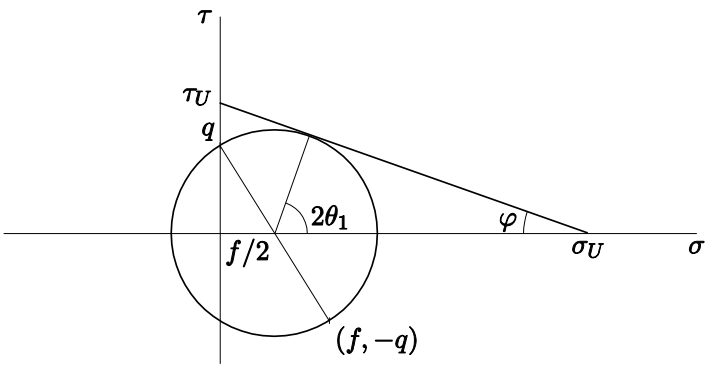

Figure 7. Morh Circle and Activation Criterion for combined bending and torsion.

Combined Bending and Torsion Test

This is a test combining bending and torsional fatigue. The normal applied stress is $f \leq b$ and the aim is to determine the minimum shear stress q required to cause fatigue failure. Figure 7 shows the Mohr circle obtained under these conditions. The point with abscissa $f/2$ in the horizontal axis is used to draw a line normal to that for the microscopic activation criterion. The intersection with such a line defines the radius of the Mohr circle. In turn, the intersection of the circle with the vertical axis determines the sought value of the shear stress, q. Accordingly, the radius of the circle defining the biaxial fatigue limit obeys the following equation:

$$\sin\varphi = \frac{\sqrt{\frac{f^2}{4}+q^2}}{\sigma_U - \frac{f}{2}} = \frac{\tau_U}{\sqrt{\tau_U^2+\sigma_U^2}} \tag{11}$$

As can be seen, substituting the previous expressions for τ_U and σ_U as a function of b and t (Eq. (10)) into Eq. (11) yields

$$\frac{q^2}{t^2} + \frac{f^2}{b^2}\left(\frac{b}{t}-1\right) + \frac{f}{b}\left(2-\frac{b}{t}\right) = 1 \tag{12}$$

which is *exactly* Eq. (2).

DISCUSSION AND CONCLUSION

It can be concluded that the proposed micromechanical model provides an accurate theoretical prediction of the ellipse arc established from the experimental data of Gough *et al.* This testifies to the usefulness of the micromechanical models for small crack propagation. However, we should note that the same equation can also be obtained by using alternative theories. In fact, Gough himself [2, p. 40] not only insisted that he adopted both the ellipse arc and ellipse quadrant based purely on the empirical evidence, but also noted that the ellipse arc had by then been predicted via three different routes. Discussing such theories is beyond the scope of this paper, however.

It must be carefully noted that the equations presented here do not apply to non-proportional loading. It is well known that non-proportional loads induce dislocation substructures far more complex than proportional loads. This is due to the production of cyclic plastic strains along multiple slip systems associated with the rotation of the principal strain axes during non-proportional cycling. Thus the simple model of a slip band of fixed orientation can hardly be expected to apply in that case.

ACKNOWLEDGEMENTS

The authors would like to thank the Spanish Ministry of Science and Innovation for its financial support through grant DPI2008-01100 and the Junta de Andalucía through TEP1752 and P07-TEP-03045.

REFERENCES

1. Gough, H.J. (1950), Engineering Steels Under Combined Cyclic and Static Stresses, *J. Appl. Mech.*, Vol. 50, pp.113-125.
2. Gough, H.J., Pollard, H.V. and Clenshaw, W.J. (1951), Some Experiments on the Resistance of Metals to Fatigue under Combined Stresses, *Ministry of Supply, Aeronautical Research Council Reports and* Memoranda, London: His Majesty's Stationary Office, 1951. 141+XII pages.
3. ANSI/ASME B106.1M-1985 Standard, *Design of Transmission Shafting*.
4. Navarro, A. y de los Rios, E.R. (1988) Short and Long Fatigue Crack Growth: a Unified Model, *Phil. Mag.*, Vol. 57(1), pp 15-36.
5. Navarro, A. y de los Rios, E.R. (1992) Fatigue Crack Growth Modelling by Successive Blocking of Dislocations, *Proc. R. Soc. Lond. A*, Vol. 437, 375-390.
6. Vallellano, C., Navarro, A. y Domínguez , J. (2000) Fatigue Crack Growth Threshold Conditions at Notches. Part I: Theory, *Fatigue Fract. Engng. Mater. Struct.*, Vol. 23, 113-121.
7. Vallellano, C., Navarro, A. y Domínguez , J. (2000) Fatigue Crack Growth Threshold Conditions at Notches. Part II: Generalization and Application to Experimental Results, *Fatigue Fract. Engng. Mater. Struct.*, Vol. 23, 123-128.
8. Navarro A, Vallellano C, de los Rios ER, Xin XJ. (1997) Notch sensitivity and size effects by a short crack propagation model. In: Engineering Against Fatigue, Proc of an International Conference, Sheffield, U K, A A Balkema Publishers, Rotterdam.
9. Chaves V, Navarro A. (2009) Application of a microstructural model for predicting notch fatigue limits under Mode I loading. Int J Fatigue; 31:943-951.